Comparison of the defective pyrochlore and ilmenite polymorphs of $AgSbO_3$ using GGA and hybrid DFT

Jeremy P. Allen,* M. Kristin Nilsson, David O. Scanlon, and Graeme W. Watson†
School of Chemistry and CRANN, Trinity College Dublin, Dublin 2, Ireland
(Received 20 October 2010; published 24 January 2011)

Silver antimonate, $AgSbO_3$, in both its defective pyrochlore and ilmenite structural polymorphs, has been suggested as a possible candidate mixed metal oxide for use in the photocatalytic splitting of water in visible light. In this study, we report electronic-structure calculations, using both standard and hybrid density-functional-theory approaches, on both structural forms of $AgSbO_3$ to fully characterize the band structure and composition of the valence and conduction bands. Analysis of conduction properties and optical absorption is also used to compare the predicted properties of the two materials. Results show that the valence band is dominated by O 2*p* and Ag 4*d* states, whereas the conduction band is composed mainly of Ag and Sb 5*s* states. Band-edge effective-mass calculations indicate the materials operate via an *n*-type mechanism, with conduction properties being comparable for the two materials. The fundamental and optical band gaps are also predicted to be compatible with visible light adsorption.

DOI: 10.1103/PhysRevB.83.035207 PACS number(s): 31.15.−p, 71.20.Mq, 71.15.Mb

I. INTRODUCTION

Over the past decade, photocatalysis has received a great deal of attention.[1–3] This has mainly been in an effort to achieve an efficient use of solar radiation to help combat issues relating to both energy production, such as the formation of H_2 from the splitting of water, and environmental concerns, such as the degradation of organic pollutants.[1,4,5]

The search for new or improved photocatalysts is never straightforward, as certain requirements in the electronic structure are needed. For example, a number of conditions are required for an efficient water-splitting material. Not only is the size of the band gap of importance, but also the positions of the band edges. The conduction-band minimum (CBM) must have a potential more negative than that of the H^+/H_2 redox potential [0 V versus normal hydrogen electrode (NHE)]. In addition, the valence-band maximum (VBM) must have a more positive potential than the redox potential of O_2/H_2O (+1.23) eV. This also provides the requirement that the very minimum theoretical band gap for a water-splitting material is 1.23 eV. To generate an effective photocatalyst that is driven by visible light, a band gap of less than 3.0 eV is also required.[1]

The first reported semiconductor for use in solar hydrogen production was anatase TiO_2,[6] and, as such, it has spawned a vast amount of research.[1,7–9] TiO_2 is also highly stable and cost-effective, however, as anatase TiO_2 has a band gap of 3.2 eV,[4] it cannot operate efficiently under visible light illumination.

One approach to improve the efficiency of TiO_2 has been through doping with nonmetallic elements, such as N and C, or metallic elements, for example Cr and V, but this approach only yields limited improvement.[10–14] Although doping offers one way to enhance the properties, investigations of alternative systems can also be instructive. One such alternative is mixed metal oxides, which have been shown to possess promising photocatalytic properties.[1,15–18]

Most mixed metal oxide photocatalysts typically contain at least two different metal cations, one of low valence (I-II) and a second of higher valence (III-VI). The higher valence metal cation possesses either d^0, such as Ti(IV), Nb(V), or W(VI), or d^{10} electronic configurations, such as Ga(III), Sn(IV), or Sb(V). This gives rise to conduction bands (CB) that are composed mainly of *d* or *s*/*p* states, respectively. As *s*/*p* electrons are less localized than *d* electrons, they are believed to give rise to a more dispersive conduction band with higher electron mobility and higher photocatalytic activity.[19,20] The low valence cation, often an alkali or alkaline earth metal element, has little influence on the top of the valence band (VB), giving rise to an O 2*p* dominated VB. However, many of the mixed metal oxides with these compositions, such as $Ca_2Nb_2O_7$, $NaTaO_3$, and $NaSbO_3$, have a band gap greater than 3 eV, making them only responsive to ultraviolet (UV) rather than visible light. To make them usable as a visible light photocatalyst, some kind of modification or band engineering is required.[1] By choosing a low valence cation that has orbitals that will mix with the O 2*p* states, such as Ag(I) 4*d* or Pb(II) 6*s* states, the energy of the valence band can be raised and the band gap decreased. An example of such a material is the photocatalyst $AgSbO_3$.[21,22]

$AgSbO_3$ has two main polymorphs, with defective pyrochlore[23] and ilmenite[24] structures. The ilmenite is metastable, only forming through low-temperature ion exchange from the isostructural $NaSbO_3$, and will undergo a phase transition to the defective pyrochlore under heat treatment.[24,25] The reported optical band gaps are 2.6 (Ref. 22) and 2.4–2.5 eV (Refs. 21 and 25) for the defective pyrochlore and ilmenite structures, respectively.

The evolution of O_2, via the photocatalytic splitting of water, in the defective pyrochlore structure has been studied by Kako *et al.*[22] The results of this study showed it to have a greater performance than WO_3, which is known to be a good photocatalyst for O_2 evolution in the presence of Ag(I) but inactive for H_2 evolution.[26] Although the defective pyrochlore was untested for H_2 evolution, this suggests that it could have a possible role as a water splitter. The authors also considered its activity toward the degradation of organic molecules, through the oxidation of 2-propanol, with results

suggesting that $AgSbO_3$ in a defective pyrochlore structure has a strong enough oxidizing potential to decompose organic compounds.

Singh and Uma[21] also looked at the potential for $AgSbO_3$ to decompose organic molecules, studying both the ilmenite and defective pyrochlore polymorphs. Their results suggested that the ilmenite is superior to the defective pyrochlore for the degradation of the organic dyes and 2-chlorophenol under visible light. The defective pyrochlore structure showed either reduced activity, or, for the 2-chlorophenol, a lack of significant activity at all. However, they did suggest that this lower activity could be related to varying stoichiometries in the samples, as the work of Kako *et al.*[22] showed that deviations away from ideal stoichiometries had a significant effect on the reactivity, with $Ag_{1.00}SbO_3 > Ag_{1.02}SbO_3 > Ag_{0.99}SbO_3$.

The reduction in reactivity with stoichiometry for the defective pyrochlore $AgSbO_3$ suggests that any defects present in the material will cause a reduction in the photocatalytic properties. For the Ag-deficient $Ag_{0.99}SbO_3$, Ag vacancies are suggested to act as centers of recombination between the photogenerated holes and electrons,[22,27] in a similar manner to that observed for $AgTaO_3$.[28] For hyperstoichiometries, $Ag_{1.02}SbO_3$, the silver excess is manifested as metallic silver, which Kako *et al.* reasoned would have a shielding effect on the surface of the material, reducing both the number of active sites for O_2 evolution and the amount of visible light it could adsorb.[22] Wang *et al.*[29] have also studied the effect of varying the Ag/Sb ratio on the photocatalytic properties. Conversely, they reported that an increase in the amount of Ag to Sb caused a reduction in the optical band gap and an increase in the photocatalytic activity, which they attributed to the formation of Sb(III) in the sample.

Kako and Ye[25] suggested that the photocatalytic properties of $AgSbO_3$ can be improved by preparing samples with mixed phases of the defective pyrochlore and ilmenite. Their results showed a greater activity than both a TiO_2 photocatalyst and the single-phase ilmenite material for the decomposition of acetylaldehyde to CO_2. They claim that the cause of this increased photocatalytic activity is a synergistic effect between the two phases, which occurs as the band edges of the ilmenite polymorph lay within those of the defective pyrochlore.

Although the primary focus on $AgSbO_3$ has been for its utilization in photocatalysis, the defective pyrochlore has also been investigated for use as an Ag(I) ion conductor,[30] an *n*-type thermoelectric material,[31,32] and as a transparent conducting oxide (TCO).[23,33]

Density-functional-theory (DFT) calculations have been previously employed by Kako *et al.*[22] and Mizoguchi *et al.*[23] to consider the electronic structure of the defective pyrochlore form of $AgSbO_3$. Both studies showed that the composition of the VB and CB are as expected, with the top of the VB consisting of a mixture of Ag 4*d* and O 2*p* states and the bottom of the CB dominated by Ag and Sb 5*s* states. The composition of the VB has also been confirmed through UV photoemission spectroscopy (UPS).[34] As expected for these computational approaches, the calculated band gaps for the defective pyrochlore structures are significantly underestimated, with reported values of 0.1 (Ref. 23) and 0.4 eV.[22]

The aim of this study is to provide a characterization of the electronic structures of both the defective pyrochlore and ilmenite forms using hybrid-DFT, which is expected to not only give a better structural representation but also to significantly improve the calculated band gap.[35–38] Calculations have also been carried out using the standard generalized-gradient approximation (GGA), allowing for a direct comparison to be made with the hybrid-DFT method. In addition, the calculation of band structures, optical absorption and the hole effective masses at both the VBM and CBM allows a quantification of the conduction properties of these materials. This not only allows comparisons to be made between the two different structures, but also a discussion of the suitability of the two materials for *n*-type water splitting.

II. COMPUTATIONAL METHODS

The calculations described in this study were all performed using the periodic DFT code VASP,[39,40] which uses a plane-wave basis set to describe the valence electrons. The projector-augmented-wave (PAW)[41,42] method was used to describe the interactions between the cores (Ag: [Kr], Sb: [Kr], and O: [He]) and valence electrons. Two methods of treating the exchange and correlation were used in this study to allow a comparison to be made of their effectiveness. The first method used the standard GGA approach with the Perdew-Burke-Ernzerhof (PBE)[43] functional. The second approach was that of Heyd, Scuzeria, and Ernzerhof (HSE06),[44,45] which uses a screened hybrid functional and includes a percentage of exact Fock exchange. The HSE06 methodology is identical to that described elsewhere, where the percentage of exact nonlocal Fock exchange added to the PBE functional is 25% and the long- and short-range parts of the functional are partitioned by a screening of $\omega = 0.11\ \text{bohr}^{-1}$.[38,46] Although hybrid functionals are more computationally demanding, they are often found to give better approximations of band gaps in semiconductor systems and improved structural data.[35,38,47–63]

The bulk equilibrium lattice parameters were determined by performing structural optimizations at a series of volumes. In each of these calculations, the atomic positions, lattice vectors, and cell angles were allowed to relax while the total cell volume was held fixed. The resulting energy-volume curves were then fitted to the Murnaghan equation of state to obtain the equilibrium bulk cell volume.[64] This approach avoids the problems of Pulay stress and changes in basis set that accompany volume changes in plane-wave calculations. The two polymorphs were modeled using their primitive unit cells, for which a Γ-centered $4 \times 4 \times 4$ *k*-point mesh was found to be sufficient for both materials. A plane-wave cutoff of 500 eV was used for the PBE calculations but reduced to 400 eV for the HSE06 due to the high computational cost.[46] For all calculations, the structures were deemed to be converged when the forces on all the atoms were less than 0.01 $\text{eV}\text{Å}^{-1}$.

The optical-absorption spectra, as well as the optical transition matrix, was calculated within the transversal approximation,[65] using an increased *k*-point mesh of $6 \times 6 \times 6$. This approach sums all direct VB to CB transitions to determine the optical absorption, thereby ignoring both indirect and intraband transitions.[66] As only single-particle transitions are included, any electron-hole correlations would require higher-order electronic-structure methods.[67,68]

However, this approach has been shown to provide reasonable optical-absorption spectra.[16,38,46,56,69]

Structural figures have been generated using the VESTA package.[70]

III. RESULTS AND DISCUSSION

A. Defective pyrochlore structure

The defective cubic pyrochlore structure, space group $Fd\bar{3}m$, is the most common form adopted by $AgSbO_3$. A typical cubic pyrochlore structure has a general formula of $A_2B_2O_6X$, where X is typically O, F, or OH.[71] The structure is composed of a corner-sharing BO_6 octahedra network, with the larger A cations possessing eightfold coordination, approaching a hexagonal bipyramid, to six O and two X anions. This AX_2 sublattice forms a channel network through the structure. The defective pyrochlore structure, exhibited by $AgSbO_3$, differs from that of a typical cubic pyrochlore in that the X anions are absent. This gives rise to sixfold-coordinated Ag ions with a distorted octahedral geometry, approximating a flattened trigonal antiprism.[72] The structure is shown in Fig. 1, with a comparison of the calculated structural parameters to the experimental structure of Mizoguchi *et al.*[23] provided in Table I. As can be seen, there is good agreement between the calculated and experimental structures, with the HSE06 functional providing a better fit to experiment as expected.

The calculated total and partial (ion decomposed) electronic densities of states (EDOS and PEDOS, respectively) for the defective pyrochlore structure are shown in Fig. 2. The EDOS can be broadly separated into four regions, with the VB comprising regions I–III and region IV representing the CB. The HSE06 calculation gives rise to a widening of the band gap and a small expansion of the VB in comparison to the PBE calculation, therefore giving slightly different widths for the different regions of the EDOS. However, similarities in the peak structure and composition are seen between the different methods. The O 2p states are seen throughout all regions in the EDOS for both methods, although the contributions from the cations are seen to differ between regions. The cation states

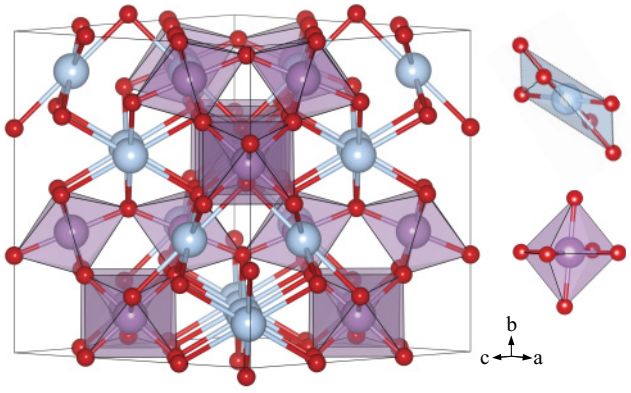

FIG. 1. (Color online) Schematic showing the optimized $AgSbO_3$ defective pyrochlore structure. Silver, antimony, and oxygen atoms are colored blue (light gray), purple (medium gray), and red (dark gray), respectively. The antimony atoms are also shown as polyhedra in the main image. Coordination environments of the AgO_6 and SbO_6 octahedra are also shown.

TABLE I. Comparison between experimental lattice constants and bond lengths for $AgSbO_3$ in the defective pyrochlore structure with those calculated using PBE and HSE06 methods. Percentage changes from experiment are given in parentheses, and all values are in Å except the cell volume, which has units of Å^3.

Property	PBE	HSE06	Experiment[23]
a	10.43(1.6)	10.31(0.4)	10.27
Volume	1134.62(6.0)	1095.91(2.4)	1083.21
Ag-O	2.59(1.6)	2.58(1.2)	2.55
Sb-O	2.01(1.5)	1.97(−0.5)	1.98
Ag-Ag	3.69(1.7)	3.65(0.6)	3.63
Ag-Sb	3.69(1.7)	3.65(0.6)	3.63
Sb-Sb	3.69(1.7)	3.65(0.6)	3.63

in regions I and II are primarily composed of Sb 5s and 5p states, respectively, with a small amount of Sb 4d states seen in region II. Region III, however, is a mixture of Ag and Sb 4d states mixing with the O 2p, with the Ag states dominating. The CB, region IV, is comprised of Ag 5s, Sb 5s and p, and O 2p.

Agreement is seen between the calculated PEDOS and experimental photoemission spectra.[34] The UPS data of Yasukawa *et al.* indicate four peaks in the upper valence band. Working back from the Fermi energy, the first three peaks were designated as being composed of Ag 4d and O 2p states, with the peak at the top of the VB having a significant contribution from the Ag 4d states. The fourth peak was described as consisting of mixed O 2p and cationic s and p states. This description is qualitatively similar to the calculated PEDOS, with Ag 4d and O 2p states dominating the upper valence band. The calculated PEDOS also suggests that the cationic s

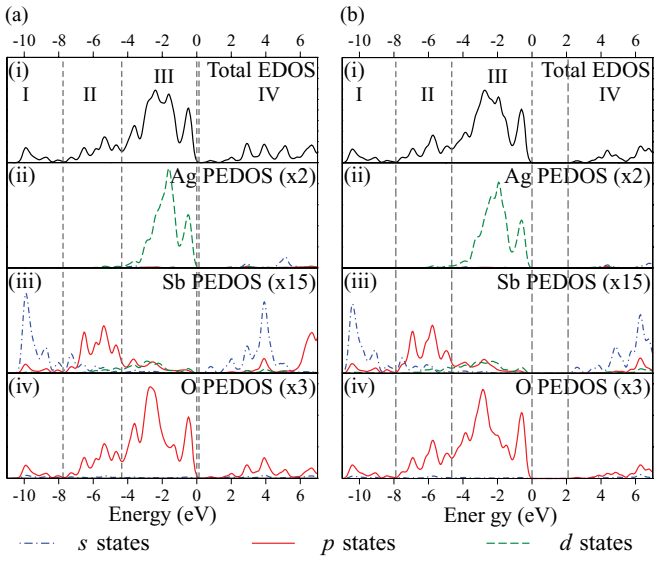

FIG. 2. (Color online) Electronic density of states for $AgSbO_3$ in a defective pyrochlore structure, split into (i) the total EDOS, (ii) Ag PEDOS, (iii) Sb PEDOS, and (c) O PEDOS, as calculated using the (a) PBE and (b) HSE06 method. The s, p, and d states are colored blue (dot-dash), red (solid), and green (dash), respectively. Vertical dashed gray lines represent divisions between different regions in the DOS. The Fermi energy has also been set to 0 eV.

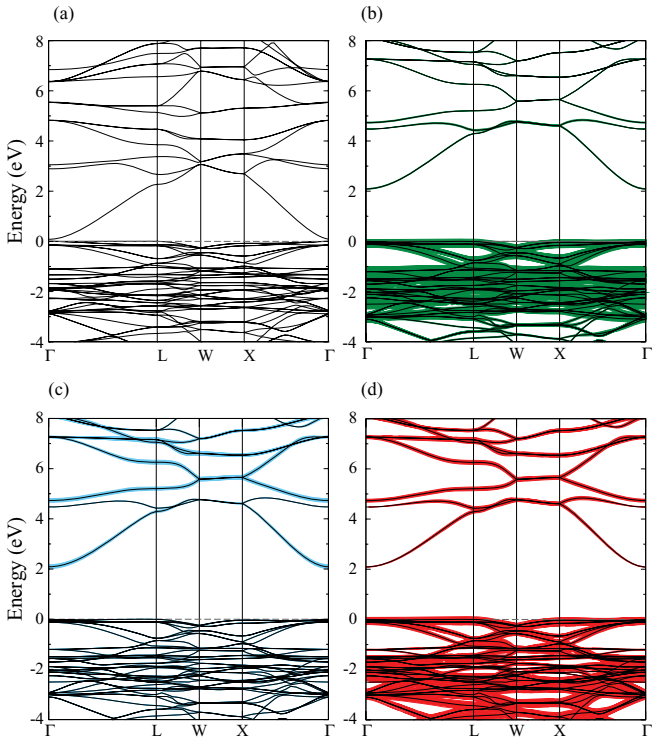

FIG. 3. (Color online) Band structure of the defective pyrochlore form of $AgSbO_3$ calculated using (a) the PBE approach and (b)–(d) the HSE06 method. The HSE06-determined band structures are shown in fatband format with the contributions to the bands from the (b) Ag 4*d* (green), (c) Sb 5*s* (blue), and (d) O 2*p* (red) states indicated. The Fermi level is set to 0 eV, as indicated by the horizontal dashed gray line.

and *p* states described for the fourth peak originate from the Sb cations, with very little contribution seen for the Ag *s* and *p* states in the valence band.

The calculated band structures for the defective pyrochlore, along the space group high-symmetry lines from Bradley and Cracknell,[73] are given in Fig. 3. The VBM is located at *L* and extends in the *L* to Γ direction for both methods, whereas the CBM is observed at the Γ point, leading to indirect band gaps of 0.08 and 2.09 eV for PBE and HSE06, respectively. The smallest direct band gaps, however, are only slightly larger at 0.09 and 2.11 eV for PBE and HSE06, respectively, and are observed at the Γ point.

For the HSE06-predicted band structure, fatband analysis has been conducted to show the contribution from the Ag 4*d*, Sb 5*s*, and O 2*p* states, Figs. 3(b)–3(d), respectively. As seen in the PEDOS, the top of the VB is dominated by mixed Ag 4*d* and O 2*p* states, with very little contribution from the Sb 5*s* states. The bottom of the CB is comprised of mainly Sb 5*s* and O 2*p* states. The contributions from Ag 5*s* states to the bottom of CB, not shown, are comparable to those of the O 2*p* states. The extent of the Sb 5*s* and O 2*p* contributions to the lowest bands in the CB are also seen to be phase-dependent. For example, at the Γ point, the primary component is seen to be from the Sb 5*s* states, however this is reversed at the W point, where O 2*p* states dominate. Although not shown, fatband analysis of the PBE-predicted band structures yields similar results. This analysis is qualitatively similar to a previous GGA study by Mizoguchi *et al.*,[23] although they report a greater mixing of Ag 5*s* states at the CBM with the Perdew-Wang functional.

B. Ilmenite structure

The ilmenite structure has a rhombohedral unit cell, space group $R\bar{3}H$, and consists of distorted octahedral AgO_6 and SbO_6 units, with the former showing the greatest distortion, exhibiting a trigonal antiprism polyhedron. The SbO_6 octahedra form edge-sharing sheets in the *ab* plane, as do the distorted AgO_6 octahedra, with the layers alternating between Ag and Sb in the *c* direction, as shown in Fig. 4. The distorted AgO_6 octahedra connect to the SbO_6 octahedra by face-sharing on one side in the *c* direction and corner-sharing in the other, with this arrangement alternating across the layer in the *ab* plane.

Comparisons between the calculated and experimental structures are given in Table II. As expected, the HSE06 method gives rise to the closest fit to experiment, with cell vectors and bond lengths within 2.1 %, whereas the PBE method predicts values within 3.0 %. However, the *c* lattice vector is seen to be expanded relative to the *a* and *b* vectors for both methods. This is more apparent in the HSE06-minimized structure as the PBE-calculated vectors also possess the typical overestimation seen for PBE calculations. Although the source of this expansion is not apparent, it may be a result of the failure of DFT (and hybrid-DFT) to account for van der Waals forces, as previously seen in the expansion of layered materials, such as SnO (Refs. 74 and 75) and V_2O_5.[76,77]

The calculated EDOS and PEDOS for the ilmenite structure are shown in Fig. 5. As with the defective pyrochlore structure, the EDOS can be broadly characterized by four regions, with

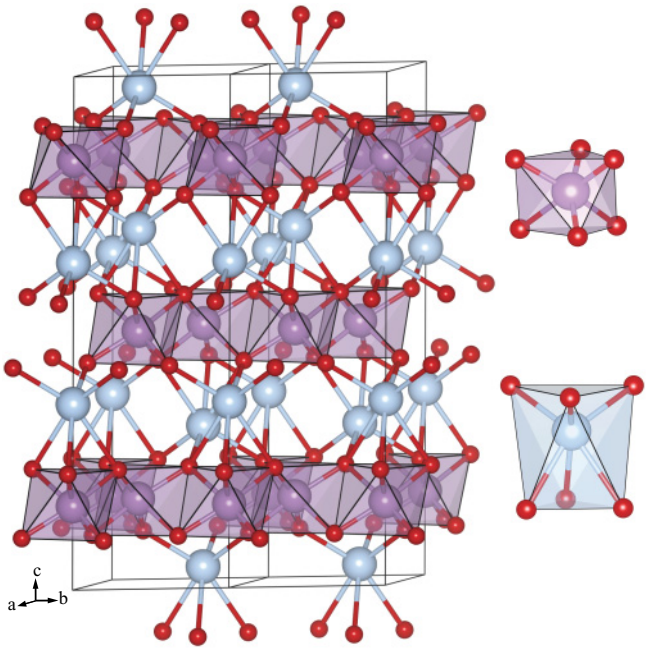

FIG. 4. (Color online) Schematic showing the optimized $AgSbO_3$ ilmenite structure. Silver, antimony, and oxygen atoms are colored blue (light gray), purple (medium gray), and red (dark gray), respectively. The antimony atoms are also shown as polyhedra in the main image. Coordination environments of the AgO_6 and SbO_6 octahedra are also shown for reference.

TABLE II. Comparison between experimental lattice constants and bond lengths for $AgSbO_3$ in the ilmenite structure with those calculated using PBE and HSE06 methods. Percentage changes from experiment are given in parentheses, and all values are in Å except the cell volume, which has units of Å^3.

Property	PBE	HSE06	Experiment[24]
a	5.42(1.7)	5.35(0.4)	5.33
b	5.42(1.7)	5.35(0.4)	5.33
c	17.05(2.1)	16.99(1.7)	16.70
Volume	500.87(5.6)	486.30(2.5)	474.43
Sb-O	2.02(2.5)	1.99(1.0)	1.97
	2.04(3.0)	2.01(1.5)	1.98
Ag-O	2.41(0.0)	2.41(0.0)	2.41
	2.75(1.5)	2.75(1.5)	2.71
Ag-Ag	3.28(2.2)	3.24(0.9)	3.21
Ag-Sb	3.40(2.7)	3.38(2.1)	3.31
Sb-Sb	3.13(1.6)	3.09(0.3)	3.08

the VB spanning regions I–III and region IV representing the CB. As expected, both the PBE- and HSE06-predicted densities of states have a number of similarities in both the peak structures and their compositions, with the primary difference being an increased band gap with the HSE06 approach. The O 2*p* states are evident throughout the VB, with the different regions being characterized by the mixing with different Ag and Sb states. The cation states are very similar to those seen for the defective pyrochlore structure, with regions I and II being composed primarily of Sb 5*s* and 5*p*, respectively. Region II also has a minor contribution from the Sb 4*d* states. Region III, however, is a mixture of Ag and Sb 4*d* states with the O 2*p*.

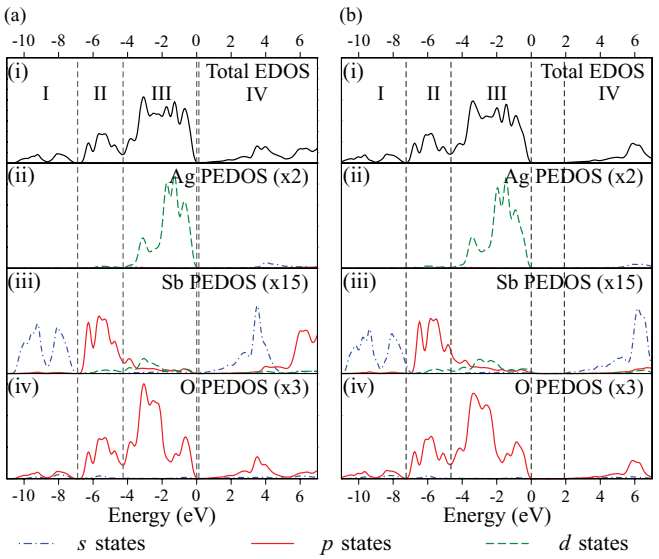

FIG. 5. (Color online) Electronic density of states for $AgSbO_3$ in an ilmenite structure, split into (i) the total EDOS, (ii) Ag PEDOS, (iii) Sb PEDOS, and (c) O PEDOS, as calculated using the (a) PBE and (b) HSE06 method. The *s*, *p*, and *d* states are colored blue (dot-dash), red (solid), and green (dash), respectively. Vertical dashed gray lines represent divisions between different regions in the DOS. The Fermi energy has also been set to 0 eV.

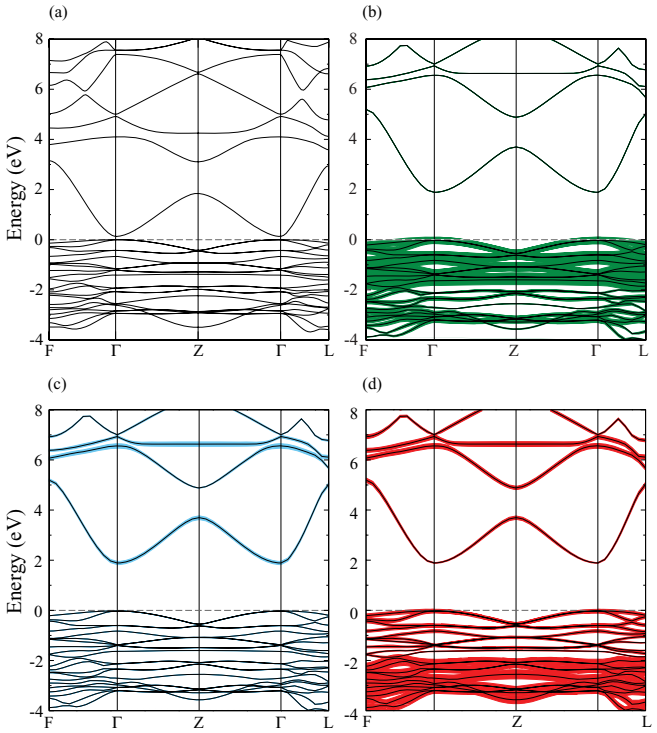

FIG. 6. (Color online) Band structure of the ilmenite form of $AgSbO_3$ calculated using (a) the PBE approach and (b)–(d) the HSE06 method. The HSE06-determined band structures are shown in a fatband format with the contributions to the bands from the (b) Ag 4*d* (green), (c) Sb 5*s* (blue), and (d) O 2*p* (red) states indicated. The Fermi level is set to 0 eV, as indicated by the horizontal dashed gray line.

The CB, region IV, is comprised of mixed Sb 5*s* and *p* with O 2*p* states.

Overall, the EDOS for the two different $AgSbO_3$ structures share a number of similarities, with the basic composition of both the VB and CB being qualitatively the same.

The band structures of the ilmenite form of $AgSbO_3$, using both PBE and HSE06 methods, are given in Fig. 6. Although both methods give rise to a similar band structure, the major difference is in the opening up of the band gap with the HSE06 method. The positions of both the VBM and CBM are the same for both methods, located at the Γ point, with direct band gaps of 0.13 and 1.92 eV for the PBE and HSE06 methods, respectively.

The HSE06-predicted band structure is shown in a fatband format, displaying the contributions from the Ag 4*d*, Sb 5*s*, and O 2*p* states in Figs. 6(b)–6(d), respectively. As expected from the PEDOS, the top of the VB is dominated by mixed Ag 4*d* and O 2*p* states, with little contribution from the Sb 5*s* states. The bottom of the CB, however, is comprised of mainly Sb 5*s* and O 2*p* states. The contribution of the Ag 5*s* states, not shown, to the lowest-energy band is similar to those seen for the Sb 5*s* states. A phase-dependent mixing of the Sb 5*s* and O 2*p* states is observed in the lowest bands in the CB. For the lowest energy band, the O 2*p* contribution is seen to decrease significantly on approaching the Γ point, whereas for the second lowest energy band in the CB, a similar case is seen for the Sb 5*s* contribution around the *Z* point. Although not

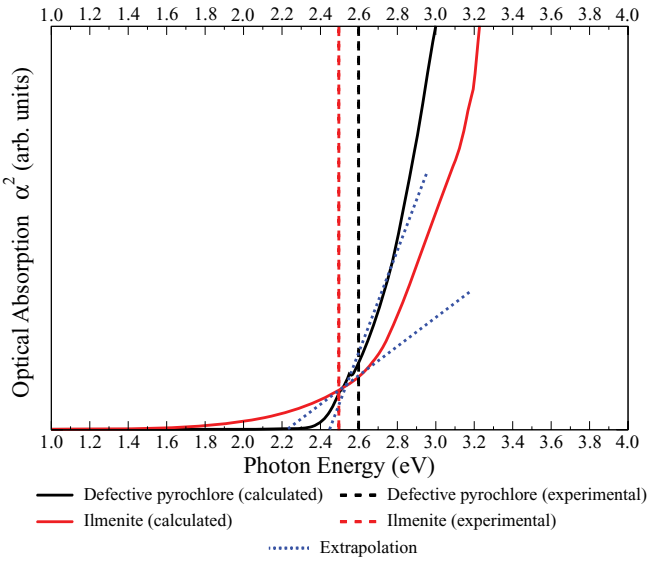

FIG. 7. (Color online) Calculated optical absorption (α^2) of the two forms of $AgSbO_3$ summed over all possible direct VB to CB transitions. Solid lines represent calculated absorption using the HSE06 method with the extrapolation used to determine the calculated optical band gap shown by the dotted lines. The experimental optical band gaps are given by the dashed lines.[21,22]

shown, fatband analysis of the PBE-predicted band structures yields similar results.

C. Optical absorption

As the experimental optical band gaps of 2.6 and 2.5 eV for the defective pyrochlore[21] and ilmenite[22] structures, respectively, are determined by optical absorption, it is instructive to compare these directly to the calculated optical absorption, rather than the fundamental band gaps. The Tauc relation states that $E_g \propto \alpha^2$, therefore, by extrapolating α^2, we can determine the value of the optical band gap. Figure 7 shows the plots of optical absorption (in terms of α^2) for both $AgSbO_3$ structures calculated using HSE06, with comparison to experiment.[21,22] The calculated optical band gaps for the defective pyrochlore and ilmenite forms are seen to be equal to 2.44 and 2.24 eV, respectively. Both the magnitudes and the relative order are consistent with experiment. The calculated optical band gaps, however, are larger than the fundamental band gaps of 2.09 and 1.92 eV for the defective pyrochlore and ilmenite, respectively.

For both materials, adsorption between the VBM and CBM at the Γ point is forbidden, which is the location of the direct fundamental band gap. The onset of adsorption for the defective pyrochlore is therefore seen along the Γ-X high-symmetry line, and along Γ-Z for the ilmenite structure. This observation is also noted for a range of oxide materials that show a symmetry-forbidden fundamental band gap, such as $CuBO_2$,[46] $SrCu_2O_2$,[78] In_2O_3,[79] and Cu_2O.[80]

D. Band-edge effective masses

To allow a comparison of the electronic conductivity of the two structures, the electron and hole effective masses at the CBM and VBM, respectively, can be determined. The effective mass (m^*) is calculated by

$$\frac{1}{m^*(E)} = \frac{1}{\hbar^2 k}\frac{dE}{dk}, \quad (1)$$

where $E(k)$ is the band-edge energy as a function of wave vector k, obtained directly from the calculation.[81] The bands at the top of the VB for both structures are clearly not parabolic, therefore $AgSbO_3$ is not expected to be well described under a typical semiconductor effective-mass approximation. However, as the bottom CB bands for the two structures are seen to be more parabolic in nature, the calculated electron effective masses should have a higher degree of accuracy than the hole effective masses. However, the calculated effective masses will serve as an approximate guide allowing comparisons to be drawn, as has been previously done for $CuMO_2$ (where M = Al, Sc, Y, Cr, and B),[82] $(Cu_2S_2)(Sr_3Sc_2O_5)$,[38] and In_2O_3,[83] indicating the relative abilities of the two structures for n- or p-type conductivity. The calculated effective masses at the VBM and CBM for the defective pyrochlore and ilmenite structures are given in Table III. Effective masses have been calculated in the [001], [010], and [100] directions, as well as along the special directions shown in the previously mentioned band structures.

TABLE III. Band-edge effective masses for the VBM and CBM of the defective pyrochlore and ilmenite forms of $AgSbO_3$, calculated with the HSE06 method. Note: For the ilmenite, the Γ-L direction is the same as the [010].

Defective pyrochlore	[001]	[010]	[100]	L-Γ	L-W	Γ-L	Γ-X
VBM	0.85	0.85	0.85	11.79	1.03		
CBM	0.26	0.26	0.26			0.26	0.26
Ilmenite	**[001]**	**[010]**	**[100]**	**Γ-F**		**Γ-Z**	
VBM	4.30	2.51	4.30	18.17		1.55	
CBM	0.27	0.27	0.27	0.28		0.29	

Table III. Effective masses have been calculated in the [001], [010], and [100] directions, as well as along the special directions shown in the previously mentioned band structures.

As can be seen, the results show that in terms of the n-type conductivity, both structures have very similar properties. The electron effective masses of the CBM are also smaller than the hole effective masses of the VBM for both structure types, indicating that the n-type ability of the materials will be greater than the p-type ability. The p-type properties differ between the structure types though, with the VBM hole effective masses suggesting that the defective pyrochlore structure will possess better p-type properties. However, neither material is predicted to exhibit strong p-type properties.

Effective-mass calculations have been used recently to describe In_2O_3, which is an industrial standard n-type TCO.[83] The effective masses at the VBM and CBM were calculated as being $16m_e$ and $0.24m_e$, respectively, and can be considered as being indicative of poor p-type and good n-type ability. The CBM electron effective masses of both $AgSbO_3$ polymorphs are comparable to In_2O_3, albeit slightly larger, suggesting that $AgSbO_3$ has strong n-type properties. Although the calculated hole effective masses of the VB are more approximate, due to its nonparabolic nature, the p-type properties will also be

significantly better than In_2O_3. Cu_2O is the parent compound of a range of *p*-type delafossite TCO's with general formula $CuMO_2$, where *M* is typically a group 3 or 13 metal. The experimental hole effective mass of the VB of Cu_2O is 0.56 m_e,[84] whereas the calculated value for the delafossite $CuBO_2$ is 0.45 m_e.[82] In comparison, our calculated VBM hole effective masses suggests that the defective pyrochlore may also exhibit reasonable *p*-type properties.

IV. CONCLUSION

In conclusion, this study has used both PBE and HSE06 DFT approaches to model the electronic structure of the defective pyrochlore and ilmenite forms of $AgSbO_3$. As expected, the HSE06 method affords a structure that has a much better fit to experiment, in terms of both the unit-cell dimensions and the bond lengths.

Despite the different structures, the orbital composition of the density of states and band structures for the two materials is similar, with orbital contributions to the bands in agreement with experiment[34] and previous calculation.[23,25] The top of the VB is composed primarily of Ag 4*d* and O 2*p* states. For the ilmenite polymorph, the O 2*p* states in the uppermost bands are slightly diminished, with respect to the defective pyrochlore, which may give rise to the increased dispersion in these bands. For the bottom of the CB, the composition is seen to be mainly mixed Ag 5*s*, Sb 5*s*, and O 2*p* states. However, there is a difference in the phase dependence of contributions to the lowest-energy conduction band. Both materials show a reduction in the O 2*p* states at the CBM, which increases in directions away from this point. For the defective pyrochlore, the Sb 5*s* contribution also has an inversely proportional relationship to those of the O 2*p*, reaching a maximum at the CBM.

Agreement between experiment and the HSE06-calculated band gaps is also seen. For the defective pyrochlore (ilmenite) structure, the HSE06 approach predicts an indirect (direct) fundamental band gap of 2.09 eV (1.92 eV) and an optical band gap of 2.44 eV (2.24 eV), which compares well with the experimental value of 2.6 eV (Ref. 22) [2.4–2.5 eV (Refs. 21 and 25)]. The calculated band gaps are also consistent with their use in photocatalytic splitting of water in visible light, which requires a band gap of between 1.23 and 3.00 eV. The magnitudes of these optical band gaps, however, exclude the use of $AgSbO_3$ as a TCO, which previous studies have suggested.

The two materials are also seen to have comparable effective masses for the CB, which would give rise to similar *n*-type properties. As the values of the effective masses are only slightly bigger than those calculated for In_2O_3,[83] their *n*-type properties are predicted to be good, which is a consequence of the strong dispersion seen at the bottom of the CB due to Sb 5*s* and O 2*p* interactions. In contrast to these results, experiment has suggested different reactivities for the two polymorphs.[21,29] However, this has been linked to differing stoichiometries rather than an inherent property of the pure materials. The defective pyrochlore is predicted to have better *p*-type ability than the ilmenite, and, while neither polymorph is predicted to be a strong *p*-type material, the defective pyrochlore may show reasonable *p*-type properties.

ACKNOWLEDGMENTS

This work was supported by Science Foundation Ireland through the Principal Investigators program (PI Grants No. 06/IN.1/I92 and No. 06/IN.1/I92/EC07). Calculations were performed on the IITAC and Lonsdale supercomputers as maintained by TCHPC, and the Stokes supercomputer as maintained by ICHEC.

*allenje@tcd.ie
†watsong@tcd.ie

[1] A. Kudo and Y. Miseki, Chem. Soc. Rev. **38**, 253 (2009).
[2] D. Ravelli, D. Dondi, M. Fagnoni, and A. Albini, Chem. Soc. Rev. **38**, 1999 (2009).
[3] U. I. Gaya and A. H. Abdullah, J. Photochem. Photobiol., C **9**, 1 (2008).
[4] M. R. Hoffmann, S. T. Martin, W. Choi, and D. W. Bahnemann, Chem. Rev. **95**, 69 (1995).
[5] A. Fujishima, X. Zhang, and D. A. Tryk, Int. J. Hydrogen Energy **32**, 2664 (2007).
[6] A. Fujishima and K. Honda, Nature (London) **238**, 37 (1972).
[7] M. Ni, M. K. Leung, D. Y. Leung, and K. Sumathy, Renew. Sust. Energy Rev. **11**, 401 (2007).
[8] K. Pirkanniemi and M. Sillanp, Chemosphere **48**, 1047 (2002).
[9] B. J. Morgan and G. W. Watson, Phys. Rev. B **80**, 233102 (2009).
[10] R. Asahi, T. Morikawa, T. Ohwaki, K. Aoki, and Y. Taga, Science **293**, 269 (2001).
[11] H. Irie, Y. Watanabe, and K. Hashimoto, Chem. Lett. **32**, 772 (2003).
[12] R. Dholam, N. Patel, M. Adami, and A. Miotello, Int. J. Hydrogen Energy **34**, 5337 (2009).
[13] H. Yamashita, M. Harada, J. Misaka, M. Takeuchi, K. Ikeue, and M. Anpo, J. Photochem. Photobiol. A **148**, 257 (2002).
[14] G. Liu, L. Wang, H. G. Yang, H.-M. Cheng, and G. Q. Lu, J. Mater. Chem. **20**, 831 (2010).
[15] M. D. Hernandez-Alonso, F. Fresno, S. Suarez, and J. M. Coronado, Energy Environ. Sci. **2**, 1231 (2009).
[16] A. Walsh, Y. Yan, M. N. Huda, M. M. Al Jassim, and S. H. Wei, Chem. Mater. **21**, 547 (2009).
[17] A. Walsh, K. S. Ahn, S. Shet, M. N. Huda, T. G. Deutsch, H. L. Wang, J. A. Turner, S. H. Wei, Y. F. Yan, and M. M. Al Jassim, Energy Environ. Sci. **2**, 774 (2009).
[18] A. Walsh, S.-H. Wei, Y. Yan, M. M. Al Jassim, J. A. Turner, M. Woodhouse, and B. A. Parkinson, Phys. Rev. B **76**, 165119 (2007).
[19] K. Ikarashi, J. Sato, H. Kobayashi, N. Saito, H. Nishiyama, and Y. Inoue, J. Phys. Chem. B **106**, 9048 (2002).
[20] N. Arai, N. Saito, H. Nishiyama, Y. Inoue, K. Domen, and K. Sato, Chem. Lett. **35**, 796 (2006).
[21] J. Singh and S. Uma, J. Phys. Chem. C **113**, 12483 (2009).
[22] T. Kako, N. Kikugawa, and J. Ye, Catal. Today **131**, 197 (2008).
[23] H. Mizoguchi, H. W. Eng, and P. M. Woodward, Inorg. Chem. **43**, 1667 (2004).

[24]V. B. Nalbandyan, M. Avdeev, and A. A. Pospelov, Solid State Sci. **8**, 1430 (2006).
[25]T. Kako and J. Ye, J. Mol. Catal. A **320**, 79 (2010).
[26]W. Erbs, J. Desilvestro, E. Borgarello, and M. Grätzel, J. Phys. Chem. **88**, 4001 (1984).
[27]B. Ohtani, R. M. Bowman, D. P. Colombo, H. Kominami, H. Noguchi, and K. Uosaki, Chem. Lett. **27**, 579 (1998).
[28]H. Kato, H. Kobayashi, and A. Kudo, J. Phys. Chem. B **106**, 12441 (2002).
[29]W. L. Wang, G. Q. Li, N. Yang, and W. F. Zhang, Mater. Chem. Phys. **123**, 322 (2010).
[30]H. Wiggers, U. Simon, and G. Schön, Solid State Ion. **107**, 111 (1998).
[31]S. Nishiyama, A. Ichikawa, and T. Hattori, J. Ceram. Soc. Jpn. **5**, 298 (2004).
[32]H.-Y. Sang and H.-F. Li, J. Alloys Compd. **493**, 678 (2010).
[33]H. Hosono, M. Yasukawa, and H. Kawazoe, J. Non-Cryst. Solids **203**, 334 (1996).
[34]M. Yasukawa, H. Hosono, N. Ueda, and H. Kawazoe, Solid State Commun. **95**, 399 (1995).
[35]J. P. Allen, D. O. Scanlon, and G. W. Watson, Phys. Rev. B **81**, 161103 (2010).
[36]C. Franchini, G. Kresse, and R. Podloucky, Phys. Rev. Lett. **102**, 256402 (2009).
[37]D. O. Scanlon, B. J. Morgan, G. W. Watson, and A. Walsh, Phys. Rev. Lett. **103**, 096405 (2009).
[38]D. O. Scanlon and G. W. Watson, Chem. Mater. **21**, 5435 (2009).
[39]G. Kresse and J. Hafner, Phys. Rev. B **49**, 14251 (1994).
[40]G. Kresse and J. Furthmüller, Phys. Rev. B **54**, 11169 (1996).
[41]P. E. Blöchl, Phys. Rev. B **50**, 17953 (1994).
[42]G. Kresse and D. Joubert, Phys. Rev. B **59**, 1758 (1999).
[43]J. P. Perdew, K. Burke, and M. Ernzerhof, Phys. Rev. Lett. **77**, 3865 (1996).
[44]S. Heyd, G. E. Scuseria, and M. Ernzerhof, J. Chem. Phys. **118**, 8207 (2003).
[45]A. V. Krukau, O. A. Vydrov, A. F. Izmaylov, and G. E. Scuseria, J. Chem. Phys. **125**, 224106 (2006).
[46]D. O. Scanlon, A. Walsh, and G. W. Watson, Chem. Mater. **21**, 4568 (2009).
[47]A. Stroppa and G. Kresse, New J. Phys. **10**, 063020 (2008).
[48]A. Stroppa and G. Kresse, Phys. Rev. B **79**, 201201(R) (2009).
[49]A. Stroppa and S. Picozzi, Phys. Chem. Chem. Phys. **12**, 5405 (2010).
[50]A. Stroppa, K. Termentzidis, J. Paier, G. Kresse, and J. Hafner, Phys. Rev. B **76**, 195440 (2007).
[51]G. Giovannetti, S. Kumar, A. Stroppa, J. van den Brink, and S. Picozzi, Phys. Rev. Lett. **103**, 266401 (2009).
[52]M. Marsman, J. Paier, A. Stroppa, and G. Kresse, J. Phys. Condens. Matter **20**, 064201 (2008).
[53]J. Heyd and G. E. Scuseria, J. Chem. Phys. **121**, 1187 (2004).
[54]J. Heyd, J. E. Peralta, G. E. Scuseria, and R. L. Martin, J. Chem. Phys. **123**, 174101 (2005).
[55]J. L. F. Da Silva, M. V. Ganduglia-Pirovano, J. Sauer, V. Bayer, and G. Kresse, Phys. Rev. B **75**, 045121 (2007).
[56]A. Walsh, J. L. F. Da Silva, Y. Yan, M. M. Al Jassim, and S. H. Wei, Phys. Rev. B **79**, 073105 (2009).
[57]S. Chen, Z. G. Gong, A. Walsh, and S. H. Wei, Appl. Phys. Lett. **94**, 041903 (2009).
[58]J. Paier, R. Asahi, A. Nagoya, and G. Kresse, Phys. Rev. B **79**, 115126 (2009).
[59]I. D. Prodan, G. E. Scuseria, and R. L. Martin, Phys. Rev. B **73**, 045104 (2006).
[60]J. E. Peralta, J. Heyd, G. E. Scuseria, and R. L. Martin, Phys. Rev. B **74**, 073101 (2006).
[61]B. G. Janesko, T. M. Henderson, and G. E. Scuseria, Phys. Chem. Chem. Phys. **11**, 443 (2009).
[62]D. O. Scanlon and G. W. Watson, J. Phys. Chem. Lett. **1**, 3195 (2010).
[63]D. O. Scanlon and G. W. Watson, J. Phys. Chem. Lett. **1**, 2582 (2010).
[64]F. D. Murnaghan, Proc. Nat. Acad. Sci. USA **30**, 244 (1944).
[65]M. Gajdos, K. Hummer, G. Kresse, J. Furthmuller, and F. Bechstedt, Phys. Rev. B **73**, 045112 (2006).
[66]B. Adolph, J. Furthmuller, and F. Bechstedt, Phys. Rev. B **63**, 125108 (2001).
[67]L. E. Ramos, J. Paier, G. Kresse, and F. Bechstedt, Phys. Rev. B **78**, 195423 (2008).
[68]J. Paier, M. Marsman, and G. Kresse, Phys. Rev. B **78**, 121201 (2008).
[69]X. Nie, S. H. Wei, and S. B. Zhang, Phys. Rev. Lett. **88**, 066405 (2002).
[70]K. Momma and F. Izumi, J. Appl. Crystallogr. **41**, 653 (2008).
[71]H. Mizoguchi, P. M. Woodward, S.-H. Byeon, and J. B. Parise, J. Am. Chem. Soc. **126**, 3175 (2004).
[72]A. W. Sleight, Mater. Res. Bull. **4**, 377 (1969).
[73]C. J. Bradley and A. P. Cracknell, *Mathematical Theory of Symmetry in Solids* (Oxford University Press, Oxford, 1972).
[74]G. W. Watson and S. C. Parker, J. Phys. Chem. B **103**, 1258 (1999).
[75]G. W. Watson, J. Chem. Phys. **114**, 758 (2001).
[76]D. O. Scanlon, A. Walsh, B. J. Morgan, and G. W. Watson, J. Phys. Chem. C **112**, 9903 (2008).
[77]D. O. Scanlon, G. W. Watson, D. J. Payne, G. R. Atkinson, R. G. Egdell, and D. S. L. Law, J. Phys. Chem. C **114**, 4636 (2010).
[78]K. G. Godinho, J. J. Carey, B. J. Morgan, D. O. Scanlon, and G. W. Watson, J. Mater. Chem. **20**, 1086 (2010).
[79]A. Walsh, J. L. F. Da Silva, S. H. Wei, C. Korber, A. Klein, L. F. J. Piper, A. DeMasi, K. E. Smith, G. Panaccione, P. Torelli, D. J. Payne, A. Bourlange, and R. G. Egdell, Phys. Rev. Lett. **100**, 167402 (2008).
[80]J. P. Dahl and A. C. Switendick, J. Phys. Chem. Solids **27**, 931 (1966).
[81]D. Segev and S. H. Wei, Phys. Rev. B **71**, 125129 (2005).
[82]D. O. Scanlon, K. G. Godinho, B. J. Morgan, and G. W. Watson, J. Chem. Phys. **132**, 024707 (2010).
[83]A. Walsh, J. L. F. Da Silva, and S. H. Wei, Phys. Rev. B **78**, 075211 (2008).
[84]J. W. Hodby, T. E. Jenkins, C. Schwab, H. Tamura, and D. Trivich, J. Phys. C **9**, 1429 (1976).